Bioorthogonal nanozymes for breast cancer imaging and therapy

Xianzhi Zhang †,‡, Yuanchang Liu †,‡, Jeerapat Doungchawee †, Laura J Castellanos-García †, Kristen N Sikora †, Taewon Jeon †,¬, Ritabrita Goswami †, Stefano Fedeli †, Aarohi Gupta †, Rui Huang †, Cristina-Maria Hirschbiegel †, Roberto Cao-Milán †, Prabin K. D. Majhi ζ, Yagiz Anil Cicek †, Liang Liu †, D. Joseph Jerry ζ, Richard W. Vachet †, and Vincent M. Rotello†.*

- † Department of Chemistry, University of Massachusetts, 710 North Pleasant Street, Amherst, Massachusetts, 01003, USA
- ‡ X. Z. and Y. L. contributed equally to this work
- ¬ Molecular and Cellular Biology Graduate Program, University of Massachusetts Amherst, 230 Stockbridge Road, Amherst, Massachusetts, 01003, USA
- ζ Department of Veterinary and Animal Science, University of Massachusetts Amherst, 661 N Pleasant Street, Amherst, Massachusetts, 01003, USA.

Abstract

Bioorthogonal catalysis *via* transition metal catalysts (TMCs) enables the generation of therapeutics locally through chemical reactions not accessible by biological systems. This localization can enhance the efficacy of anticancer treatment while minimizing off-target effects. The encapsulation of TMCs into nanomaterials generates "nanozymes" to activate imaging and therapeutic agents. Here, we report the use of cationic bioorthogonal nanozymes to create localized "drug factories" for cancer therapy *in vivo*. These nanozymes remained present at the tumor site at least seven days after a single injection due to the interactions between cationic surface ligands and negatively charged cell membranes and tissue components. The prodrug was then administered systemically, and the nanozymes continuously converted the non-toxic molecules into active drugs locally. This strategy substantially reduced the tumor growth in an aggressive breast cancer model, with significantly reduced liver damage compared to traditional chemotherapy.

Keywords: Bioorthogonal catalysis, bioorthogonal nanozymes, nanocatalysts, prodrug activation, pro-fluorophore activation, anticancer therapy, LA-ICP-MS imaging

^{*}Correspondence: rotello@chem.umass.edu

1. Introduction

Local administration of chemotherapeutics enhances their anticancer efficacy by increasing the drug dose at the tumor site, which reduces off-target effects that occur with systemic administration. ^{1, 2} The direct injection of chemotherapeutics at the tumor site is commonly used, however, this method can be limited by the diffusion and rapid clearance of drugs from the injection site.³ Implanted reservoirs can be used to provide controlled localized drug delivery, however, immune rejection and fibrosis around the implants are challenges for therapeutic application.^{4, 5}

Nanostructured drug release systems offer a versatile alternative for the localized release of therapeutics, creating "drug reservoirs" directly at the target site.⁶⁻¹⁴ The slow diffusion of drug molecules from the depot enables a constant supply of therapeutics, minimizing side effects arising from systematic drug dosing.^{3, 15}

Bioorthogonal catalysis is an emerging tool that can extend the concept of drug reservoirs to "drug factories" using chemical reactions that cannot be carried out by natural enzymes. ¹⁶⁻¹⁹ Bioorthogonal transformations enable the localized and sustained generation of imaging and therapeutic agents. ²⁰⁻²³ Transition metal catalysts (TMCs) are excellent candidates for the bioorthogonal activation of prodrugs, ²⁴⁻²⁷ offering high versatility and reactivity. ²⁸⁻³⁸ However, the direct use of free TMCs in living systems is challenging due to the lack of water solubility, ^{39,40} catalyst deactivation by biomolecules, ⁴¹ and cytotoxicity of the free metals. ¹⁸

Encapsulating TMCs into nanomaterials yields bioorthogonal 'nanozymes' that enhance the solubility, stability, and biocompatibility of the catalysts.^{20, 42-47} Additionally, encapsulation extends the useful lifetime of catalysts in complex bioenvironments.⁴⁰ Moreover, through appropriate engineering of the nanoscaffold, nanozymes can be localized at therapeutically important targets.^{33, 36, 48-51} Researchers have recently demonstrated the efficacy of the bioorthogonal approach by using nanostructures to distribute catalyst sites in the tumor and performing the drug activation *in situ*. ⁵²⁻⁵⁶

We hypothesized that nanozymes with cationic surfaces would localize at injection sites, providing in situ generation of therapeutic (Figure 1). Nanozymes were fabricated through the encapsulation of TMCs into the monolayer of a cationic-functionalized gold nanoparticle to provide protection of the catalyst and adherence to tissue at the tumor site (Scheme 1). The resulting nanozymes ^{57, 58} demonstrated prolonged catalytic activity over seven days. Consequently, a single dose of nanozyme enabled intratumoral uncaging of propargyl-protected imaging profluorophores and prodrugs over an extended time (Scheme 1b). These nanozymes remained

localized at the injection site in the tumor, activating systemically injected pro-fluorophores and prodrugs. Active drugs and dyes spread from this site throughout the entire tumoral area, with limited spreading to the surrounding healthy tissue (Figure 1). Localized generation of chemotherapeutic 5-fluorouracil (5FU) from a caged prodrug provided essentially identical therapeutic efficacy to systemically-administered 5-FU. Significantly, no liver damage was observed with the localized generation of 5FU, in sharp contrast to the damage observed with systemic administration of the free drug. Taken together, nanozyme-based local generation of chemotherapeutic 5-FU efficiently treats aggressive breast cancer, without the acute hepatoxicity observed in traditional chemotherapy.

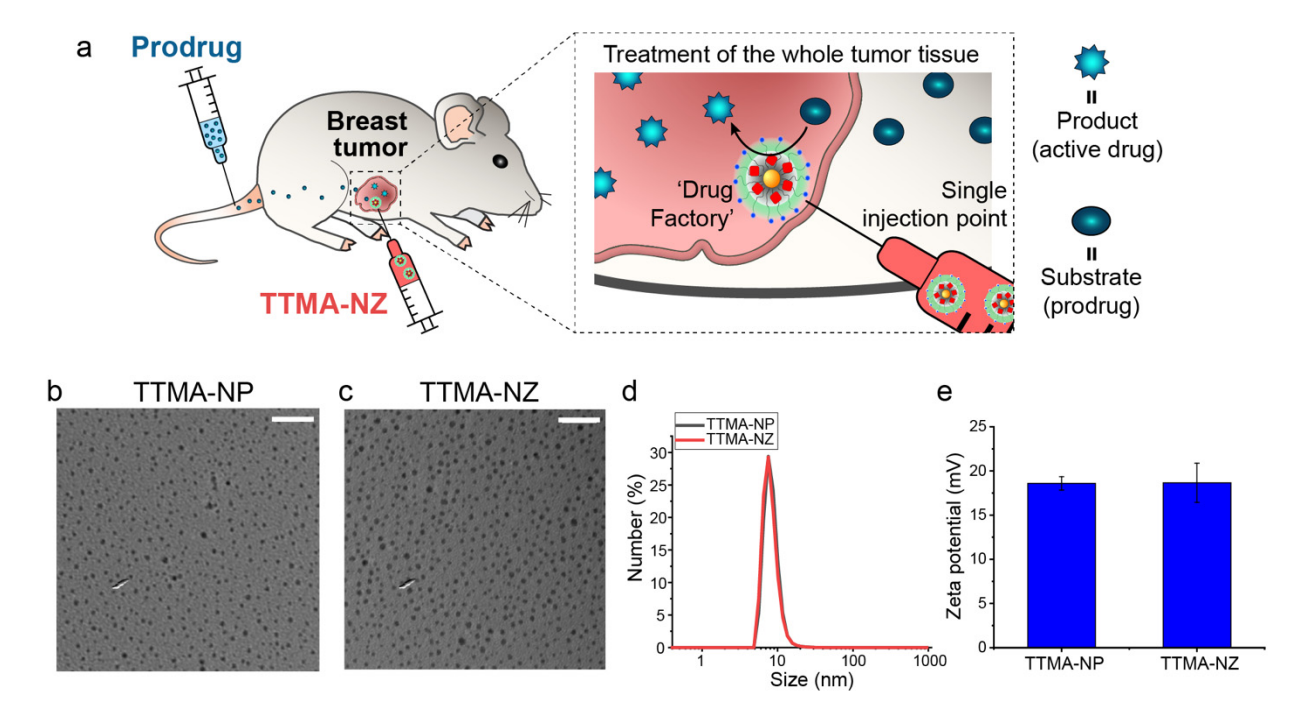


Figure 1. (a) Schematic presentation of localized therapy through *in situ* drug activation by bioorthogonal nanozymes (**TTMA-NZ**). (b) Transmission electron microscopy (TEM) image of thioalkyl tetra(ethylene glycol) trimethylammonium functionalized gold nanoparticles (**TTMA-NP**). (c) TEM image of nanozyme **TTMA-NZ** after encapsulation. Scale bar = 20 nm. (d) Dynamic light scattering of **TTMA-NP** and **TTMA-NZ**. (e) Zeta potential of **TTMA-NP** and **TTMA-NZ**. Each bar represents the average of three replicates, and the error bar represented the standard deviation.

2. Materials and methods

2.1 Encapsulation of catalysts into the monolayer of AuNPs

The palladium catalyst (0.8 mg) was dissolved in 1 mL 1:1 (v/v) acetone/ tetrahydrofuran (THF) solution and added to 13 mL aqueous solution containing \sim 1 μ M TTMA-NPs. The solution was filtered by a 0.22 μ m PES syringe filter and applied to a centrifugation filter with a 10k

molecular cut-off to remove the excess catalyst, with filtration repeated eight times to obtain the nanozyme solution. The concentration of nanozymes was determined by the absorbance at 506 nm.

2.2 Pro-Rho activation in living cells by nanozymes

HeLa cells were seeded in confocal dishes at 80k per dish 12 h prior to experiments. During the experiments, cells were treated with 2mL cell culture media containing 300 nM nanozymes for 24 h, followed by four times washing to fully remove the excess nanozymes. Fresh media containing 50 μM **pro-Rho** was added directly (mentioned as day1), or after another 24 h incubation (day 2), or after another 48 h incubation (day 3). Cell only and 50 μM **pro-Rho** only were used as negative controls. One day later, cells were stained using Hoechst 33342, washed by PBS, and imaged under Nikon A1 spectral detector confocal microscope (A1SP) using 40x lens. Green channel, excitation = 488 nm and emission = BP 505–530 nm; blue channel, excitation = 402 nm and emission = BP 450–465 nm (BP = band-pass).

After confocal imaging, cells were harvested and resuspended in PBS for flow cytometry analysis on FACS LSR II (BD Biosciences). Cells suspensions were analyzed under the same parameter setting, and 10,000 events were analyzed for each sample.

2.3 Intracellular pro-5FU activation

Cells (HeLa or HepG2) were seeded in 96 well plates at the density of 7k per well one day prior to experiments. Then, cells were treated with 500nM nanozymes for 24 h. On the next day, cells were washed with PBS four times and incubated with 0, 10, 50, 100, 200, and 500 µM **pro-5FU** for 72 h. The same concentration of **pro-5FU** and **5FU** was used as negative control and positive control, respectively. Afterward, cells were washed with PBS three times to fully remove the dead cells. Cell viability was determined by the Alamar Blue assay.

2.4 Animal care

All animal experiments were conducted according to the animal protocol (#182) approved by the Institutional Animal Care and Use Committee (IACUC) at the University of Massachusetts Amherst. Female BALB/c mice (at least 6-week-old) were purchased from the Jackson Laboratory (Bar Harbor, ME) and housed in controlled climates (22 ± 2 °C temperature, 12 h light/dark daily cycle) with free access to food and water. All mice were allowed to rest for at least one week in the animal facilities before any procedure was performed.

2.5 In vivo and ex vivo imaging of pro-HCA activation

4T1 cells (10μL, 100k) were transplanted to the mammary fat pad of the BALB/c mice. The tumor size was monitored by a caliper. Tumor volume (mm³) was calculated by the following

equation: (long diameter \times short diameter²)/2. When the tumor size reached \sim 200 mm³, nanozymes (4 μ M) in 50 μ L PBS or PBS alone (negative control) were injected into the tumor. On the next day, 100 μ L of 200 μ M **pro-HCA** in body-temperature PBS was injected through the tail vein. 24 h later, mice were shaved and imaged by IVIS using fluorescence pair at 710 nm (excitation) and 760 nm (emission). Afterward, mice were euthanized with CO₂. Blood and major organs (tumor, liver, spleen, heart, lung, brain, and kidneys) were collected and imaged by IVIS using fluorescence pair at 710 nm (excitation) and 760 nm (emission).

2.6 In vivo anticancer therapy by nanozymes

4T1 cells (10μL, 100k) were transplanted to the mammary fat pad of the BALB/c mice. When the tumor size reached ~ 100 mm³, mice were randomly divided into 5 groups. Nanozymes (4μM) in 50 μL PBS or PBS alone (negative control) were injected intratumorally on day 0. **5FU** (5mg/kg, positive control), **pro-5FU** (25mg/kg), or PBS (negative control) were injected on day 1, day 3, and day 5. Mouse body weight and tumor volume were recorded in a blind fashion on day 0 and days 2-10. Mice were euthanized with CO_2 when the tumor volume was over 1000 mm³. After sacrificing the mice, blood was collected for the liver panel assay, while tumors were weighed by an electric balance. Afterward, tumors were kept in liquid nitrogen for further LA-ICP-MS analysis.

2.7 LA-ICP-MS imaging

LA-ICP-MS images of ¹⁹⁷Au, ¹⁰⁶Pd, ⁶⁶Zn, and ⁵⁷Fe were acquired on a CETAC LSX-213 G2 laser ablation system coupled with a Perkin Elmer NexION 300x ICP-MS instrument. The following laser parameters were used: 50 µm spot size, 19 µm/s scan rate, 3.65 J laser energy, 10 Hz laser frequency, and a 10 s shutter delay. The helium carrier gas from the laser ablation system was set to 0.6 L/min.

2.8 LA-ICP-MS image processing

LA-ICP-MS images were reconstructed, analyzed, and segmented using a custom Python script RecSegImage-LA, that is freely available at GitHub (https://github.com/Vachet-Lab/RecSegImage-LA).⁵⁹ Images were rendered and overlayed using ImageJ.

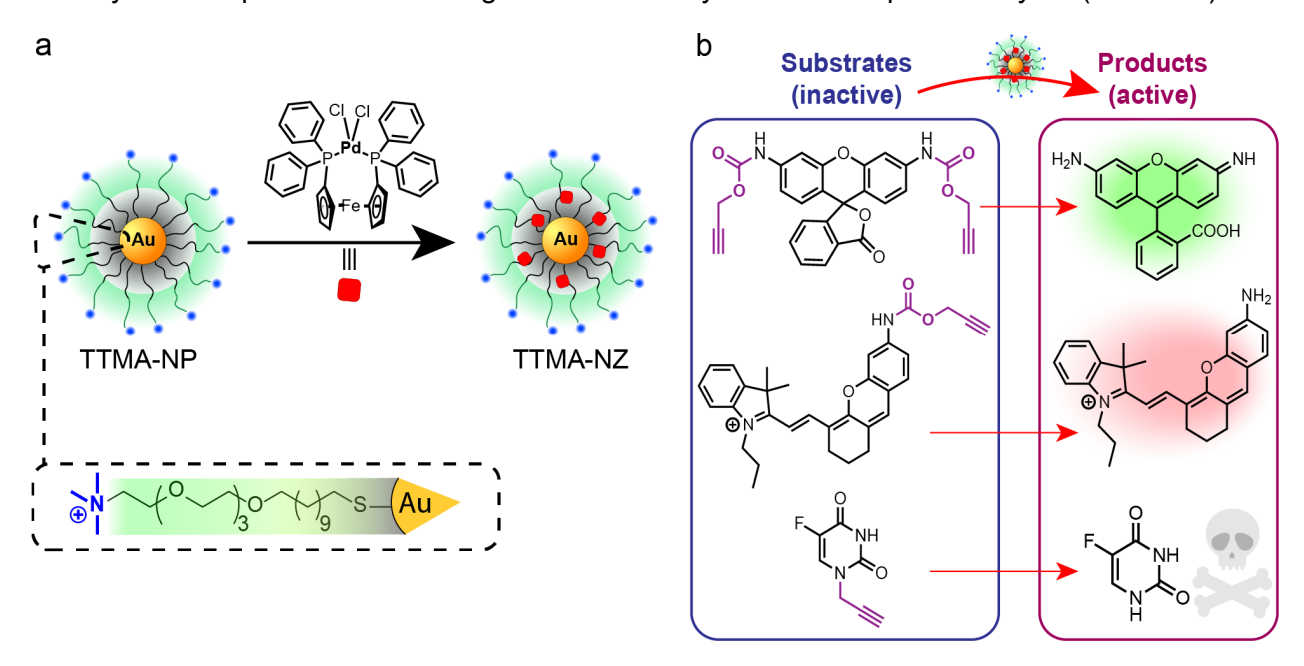
3. Results and discussion

3.1 Design and synthesis of nanozymes

The nanoparticle scaffolds used in this study were comprised of an ultrasmall (2 nm) gold core functionalized with a monolayer featuring positively charged thioalkyl tetra(ethylene glycol)

trimethylammonium ligands (**TTMA**, Scheme 1a, synthesis in supporting information Figure S1-3). The design of the ligands contains three key components: 1) a hydrophobic alkyl chain to stabilize the nanoparticles and encapsulate the catalyst molecules shown to provide nanoparticles stable in cells,⁶⁰ 2) a tetra (ethylene glycol) spacer to improve water solubility and biocompatibility, 3) a quaternary ammonium terminal group to enhance cell uptake and tumor retention.⁶¹⁻⁶³ The resulting nanoparticle (**TTMA-NP**) has low immunogenicity *in vivo*.⁶⁴⁻⁶⁶

Nanozymes (**TTMA-NZ**) were generated by encapsulating a palladium catalyst into the monolayer of AuNPs through the hydrophobic interaction *via* nanoprecipitation. A palladium ferrocene catalyst Pd(dppf)Cl₂ ([1,1'-bis(diphenylphosphino)ferrocene] dichloropalladium (II), Scheme 1a) was chosen because of its hydrophobicity and high catalytic activity.⁶⁷ Transmission electron microscopy (TEM) images and the dynamic light scattering (DLS) of **TTMA-NP** and **TTMA-NZ** indicated no aggregation after catalyst encapsulation (Figure 1 b-e). Inductively-coupled plasma mass spectrometry (ICP-MS: ¹⁰⁶Pd and ¹⁹⁷Au) verified the presence of Pd in the nanozyme and quantified an average of 28 Pd catalyst molecules per nanozyme (Table S1).



Scheme 1. Structure of nanozymes, substrates, and products. **(a).** Structure of the nanoparticle **(TTMA-NP)** and nanozyme **(TTMA-NZ)**. **(b).** Chemical structures of substrates and products. Rhodamine **(Rho)**, hemicyanine **(HCA)**, and 5-fluorouracil **(5FU)** were caged with propargyl groups to form non-fluorescent **(pro-Rho** and **pro-HCA)** and non-toxic **(pro-5FU)** substrates. Substrates are converted to fluorescent and therapeutic products by bioorthogonal nanozymes.

The catalytic activity of **TTMA-NZ** was quantified by the activation of the non-fluorescent pro-dyes (Figure 2) in phosphate-buffered saline (PBS, pH=7.4). Rhodamine 110 (**Rho**) and near-

infrared hemicyanine (**HCA**)⁶⁸ dyes were caged using a propargyl carbamate group to yield non-fluorescent pro-rhodamine (**pro-Rho**) and pro-hemicyanine (**pro-HCA**), respectively (synthesis in supporting information Figure S4-9). Fluorescence generation occurred immediately after the addition of **TTMA-NZ** to the pro-dye solution, while negative controls showed no detectable fluorescence change (Figure 2).

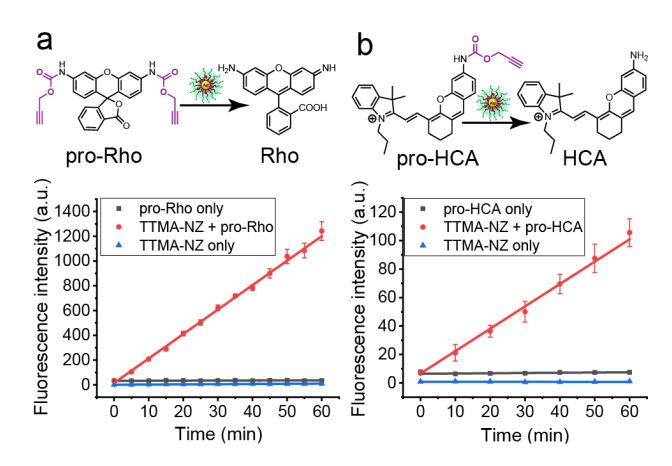


Figure 2. The catalytic activity of nanozymes (TTMA-NZ) in PBS solution. Structure and kinetic study of **(a) pro-Rho** (10 μ M) and **(b) pro-HCA** (10 μ M) activation by **TTMA-NZ** (300 nM) in phosphate-buffered saline (PBS, pH=7.4) at 37 °C. Experiments were performed in triplicate, error bars represented the standard deviation.

3.2 In vitro catalytic activity and stability of nanozymes

We next studied the catalytic activity of **TTMA-NZ** in live cells. Nanozymes showed minimal toxicity to HeLa cells at concentrations up to 800 nM (Figure S10). The cellular uptake of **TTMA-NZ** was measured by tracking ¹⁰⁶Pd and ¹⁹⁷Au with ICP-MS at different time points. The uptake of Au and Pd showed a time-dependent increase over the tested period, indicating the efficient cell internalization of these positively charged nanozymes (Figure S11).

The capability of nanozymes to perform bioorthogonal catalysis was determined by the intracellular uncaging of non-fluorescent **pro-Rho** to generate fluorescent **Rho**. HeLa cells were incubated with 300 nM nanozyme for 24 h, followed by washing four times with PBS, a protocol shown to fully remove non-internalized nanoparticles. ⁶⁹ **Pro-Rho** (50 µM) was administered after 1, 2, and 3 days (timeline in Figure 3a), and then incubated for an additional 24 h. Confocal images indicated that **TTMA-NZ** successfully activated **pro-Rho** in cells and maintained efficient catalysis over each of the incubation periods (Figure 3b-c). Flow cytometry analysis (Figure 3d) showed consistency in the fluorescence activation, confirming the retention of intracellular **TTMA-NZ** activity over a prolonged time. Consistent results were observed with **TTMA-NZ** uncaging of **pro-**

HCA, indicating the utility of this pro-fluorophore for the in vivo imaging studies below (Figure S12).

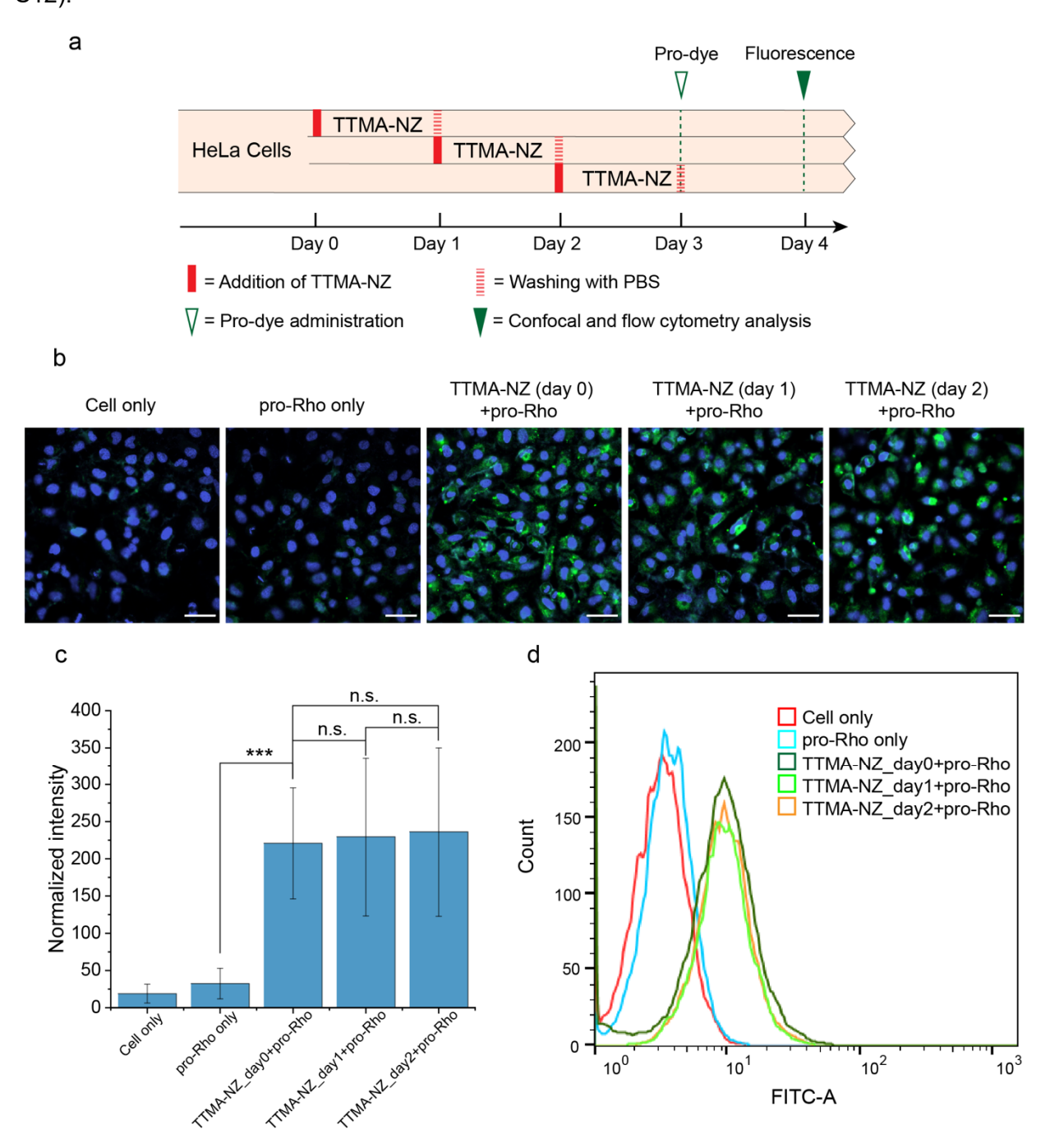


Figure 3. Nanozyme Pro-Rho activation in living cells. **(a)** Timeline of intracellular **pro-Rho** activation. **(b)** Confocal images of cells treated with a 50 μ M solution of **pro-Rho** at different time points after **TTMA-NZ** administration. The nucleus was stained by Hoechst 33342. Scale bar = 50 μ m. Nanozymes showed prolonged catalytic activity in living cells. **(c)** Quantification of intracellular fluorescence intensity of the confocal images by ImageJ software. Error bars represent standard deviation. Statistical significance was determined by a two-tailed Student's t-test. ***= p < 0.001. n.s. = not significant. **(d)** Flow cytometry of the cells. The result confirmed the stability of the nanozyme catalyst, with no change in activity observed after three days of incubation.

3.3 Intracellular drug activation by nanozymes

The ability of nanozymes to activate a caged analog of 5-fluorouracil (**5FU**) was next demonstrated. **5FU** is a highly effective chemotherapeutic, ⁷⁰ however, side effects of **5FU**, specifically liver damage, ^{71,72} can severely impact the overall health and recovery from cancer therapy. ⁷³ The **pro-5FU** was synthesized by blocking the pharmacophore with a propargyl group (synthesis in supporting info, Figure S13 and S14), ^{40, 74} resulting in an over 100-fold reduction in toxicity relative to **5FU** (Figure S15). In the presence of nanozymes, the propargyl bond is cleaved, generating the active drug **5FU** (Figure 4a). HeLa cells were pre-treated with **TTMA-NZ** for 24 h, followed by washing four times to fully remove non-internalized nanozymes. ⁶⁹ Cells were then incubated with **pro-5FU** (0-500 µM) for 72 hours. Finally, the cell viability was determined using an Alamar Blue assay. Efficient cell killing was found for cells treated with a combination of nanozymes and **pro-5FU**, providing efficacy comparable to free **5FU** treatment (Figure 4b). As expected, **pro-5FU** alone showed little toxicity to cancer cells. Comparable results were obtained when we applied experiments to liver cancer HepG2 cells (Figure S16) and murine breast cancer 4T1 cells (Figure 5c).

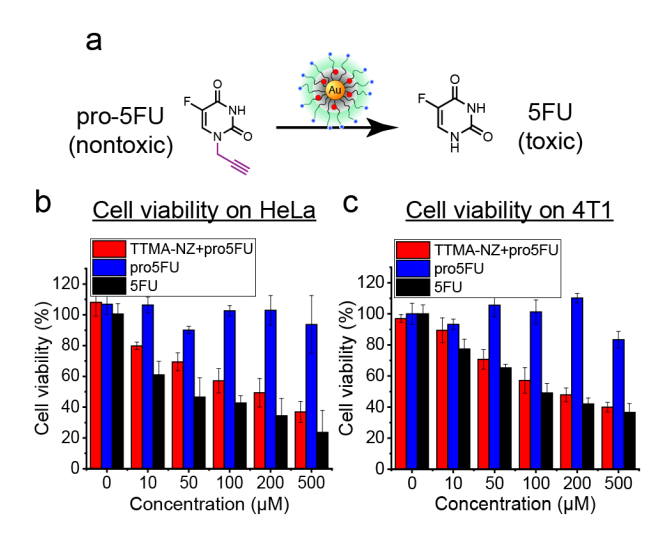


Figure 4. Intracellular drug generation by nanozymes. **(a)** Nontoxic **pro-5FU** was uncaged to chemotherapeutic **5FU** by nanozymes. **(b and c)** Cell viability of HeLa cells **(b)** and 4T1 cells **(c)** after **pro-5FU** (from 0 to 500 μ M) activation by **TTMA-NZ** (500nM for HeLa and 300nM for 4T1) for 72h. Cells treated with **pro-5FU** were used as the negative control, showing non-toxicity to cells. Experiments were performed in triplicate; error bars represent the standard deviation.

3.4 Stability and catalytic activity of nanozymes in vivo

Localization and stability are key metrics for *in vivo* activity, and were determined through intratumoral injection of nanozymes into a 4T1 orthotopic mouse model. This cancer model was established by orthotopically transplanting triple-negative 4T1 murine breast cancer cells into the mammary pad to mimic a native cancer environment. 75 The mice were sacrificed ten days after the injection. The biodistribution of nanozymes as a function of surface charge was investigated using ICP-MS, tracking both gold and palladium. The cationic nanozyme exhibited greater retention at the tumor site compared to zwitterionic and anionic nanozymes (Figure S17). The excised tumor was then cryo-sectioned into adjacent slices for imaging analysis (Figure 5a).⁷⁶ Optical imaging (Figure S18) and hematoxylin and eosin (H&E) staining provided the area and shape of the sectioned tumor slice (Figure 5b). The adjacent slice was then analyzed using laser ablation inductively coupled plasma imaging (LA-ICP-MS) to image the distribution of Au from the nanoparticle core and Pd from the catalysts encapsulated in the ligand monolayer. The signal of Au obtained by LA-ICP-MS (Figure 5c and Figure S19) co-localized with the signal of Pd (Figure 5d, e), indicating that the core and catalyst remained co-localized at the site of injection for at least ten days. The durability can be attributed to the protection of the catalyst by the metal and anchorage of the cationic particle to the tissue at the injection site.

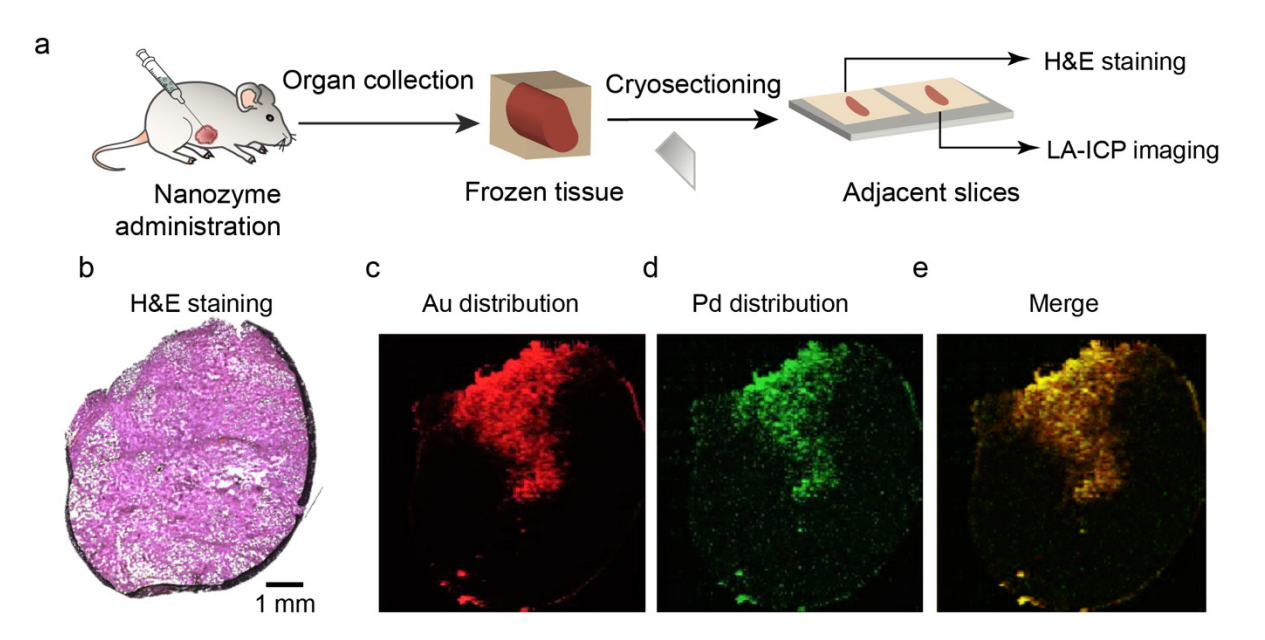


Figure 5. Representative optical and laser ablation inductively coupled plasma imaging (LA-ICP-MS) of nanozyme-injected breast tumor after 10 days. (a) Workflow of LA-ICP-MS and H&E imaging to establish nanozyme localization. (b) Histological image of the adjacent tissue section. Reconstructed LA-ICP-MS image at 50 μm resolution of (c) gold, (d) palladium, and (d) overlay. The essentially complete colocalization of Au and Pd is consistent with long-term nanozyme stability.

3.5 In vivo imaging studies

We next performed *in vivo* imaging of nanozyme activity through the uncaging of **pro-HCA** by nanozymes. After the 4T1 tumor grew to ~200 mm³, **TTMA-NZ** (50 μ L of 4 μ M) was injected intratumorally. For the imaging study, 100 μ L of a 200 μ M solution of **pro-HCA** was injected through the tail vein 24 h after nanozyme injection (Figure 6a). The mice were shaved 24 h after **pro-HCA** administration for *in vivo* imaging and then sacrificed for *ex vivo* imaging. The fluorescence signal was distributed through the entire tumor (Figure 6b, c, and Figure S20), indicating that the nanozymes maintained their catalytic activity in living animals. The observed fluorescence was limited to the tumor tissue, indicating the successful localized activation of the pro-fluorophore by **TTMA-NZ**. The results indicate efficient product diffusion throughout the tumoral tissue without affecting the surrounding healthy tissue. **Pro-HCA** alone, as expected, exhibited no fluorescence anywhere in the body and organs.

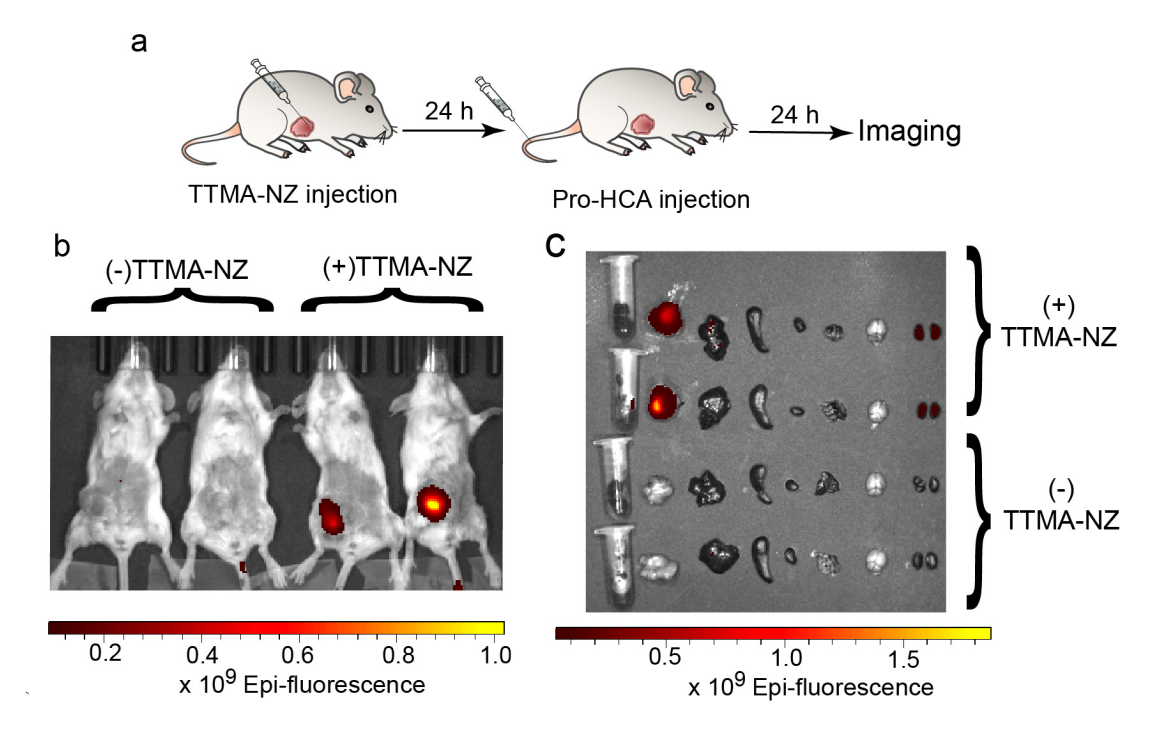


Figure 6. *In vivo* and *ex vivo* imaging of nanozyme near-infrared pro-dye activation. **(a)** Workflow of *in vivo* imaging by **pro-HCA** activation using nanozymes. **(b and c)** The activation of **pro-HCA** by nanozymes on tumor-bearing mice *in vivo* **(b)** and *ex vivo* **(c)** was demonstrated using an IVIS system. Selected organs were (from the left) blood, tumor, liver, spleen, heart, lung, brain, and kidney. The activation of the fluorophore is observed within the tumor tissue.

3.6 In vivo anticancer treatment

We next evaluated the *in vivo* anticancer efficiency of **pro-5FU** activation using **TTMA-NZ**. Tumor-bearing mice (tumor size ~100 mm³) were randomly divided into five groups that were then independently treated with (1) **TTMA-NZ+pro-5FU**, (2) **TTMA-NZ**, (3) **pro-5FU**, (4) **5FU**, and (5)

PBS. The nanozymes were injected intratumorally only once on day 0, while **pro-5FU** or **5FU** were injected intravenously on day 1, day 3, and day 5 for each of the testing groups (Figure 7a). No significant weight loss was observed for any group, indicating the absence of acute physiological effects. (Figure S21). Tumor volume was measured by a caliper and quantified in a blinded experiment. Notably, **TTMA-NZ+pro-5FU** treatment successfully reduced the tumor growth by 40% by volume and by weight compared to the PBS control group. Significantly, the efficacy of nanozyme-based drug therapy was comparable to that of the free drug group (Figure 7a and b), with both demonstrating good efficacy against the highly invasive 4T1 tumor. As expected, the treatment of **pro-5FU** alone and **TTMA-NZ** alone showed no significant difference with respect to the untreated group (Figure 7a, b, and Figure S22).

The liver is responsible for 90% of **5FU** metabolism,⁷¹ and hepatic damage is the most common side effect of 5FU-based chemotherapy.⁷³ During liver injury, the enzyme aspartate transaminase (AST) is released from the liver into the bloodstream, with the level of AST reflecting liver injury.⁷⁷ Mice treated with **5FU** expressed a much higher level of AST (Figure 7c) compared to the control groups, indicating the presence of **5FU-induced** liver damage. The mice that received **TTMA-NZ+pro-5FU**, however, exhibited no significant increase in AST relative to the negative control groups. This decrease in a key off-target effect is indicative of more directed and less harmful chemotherapy strategies driven by nanozyme-mediate bioorthogonal chemistry.

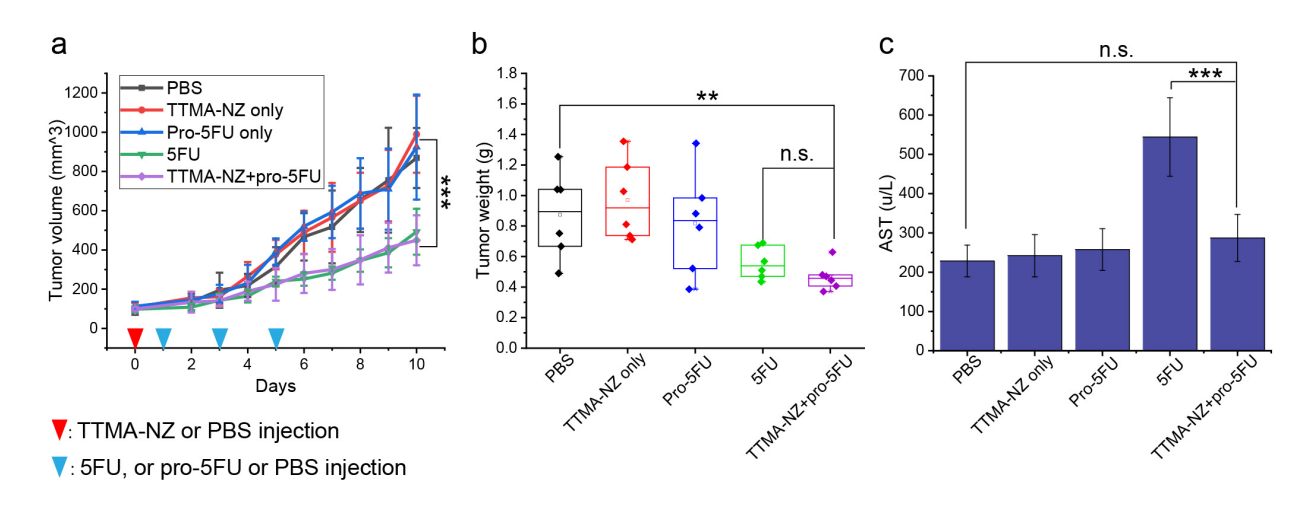


Figure 7. *In vivo* **cancer therapy using nanozymes. (a)** Change in average tumor size of experimental group and control groups. Nanozymes were injected intratumorally once on day 0 (red triangle), and **pro-5FU** was injected intravenously on day 1, 3, and 5 (blue triangle). **(b)** Final tumor mass after the treatment. **(c).** The blood of tumor-bearing mice was analyzed for liver damage (aspartate aminotransferase (AST) activity assay). **5FU**-treated mice showed a significantly higher AST level compared to the control groups and **TTMA-NZ+pro-5FU**, indicating the presence of liver damage. Nanozyme-based therapy, on the other hand, avoided the off-target effect of conventional chemotherapy. For **(a)**, **(b)** and **(c)**, data were means \pm SD, n=6. Statistical significance was determined by a two-tailed Student's t-test. **= p < 0.01, ***= p < 0.001. n.s. = not significant.

4. Conclusion

In this work, bioorthogonal nanozymes were used to provide efficient *in situ* generation of chemotherapeutics. These nanozymes provided tumor reduction equally effective to the free drug with substantially reduced off-target liver damage. This nanozyme strategy encapsulates transition metal catalysts into the monolayer of cationic gold nanoparticles. Surface engineering of the nanozyme provides long-term attachment to the intratumoral site of injection. The effective encapsulation of the TMCs in the monolayer scaffold of the nanozymes maintained high catalytic activity after injection. A single injection of nanozyme provided efficient intratumoral uncaging of systemically-administered non-toxic prodrugs into anticancer drugs. The anti-tumor efficacy of the nanozyme regimen is comparable to that observed using the systemically-administered drug. Significantly, the nanozyme treatment produced substantially less liver damage than the free therapeutic. Our obtained results show the potential of bioorthogonal nanocatalysis for the generation of therapeutically active agents. Furthermore, the modularity of the system allows for the development of stimuli-responsive and tumor-targeting nanozymes for the creation of "smart" treatment strategies. In addition to direct treatment of tumors, this approach can potentially be adapted for adjuvant therapy after surgical resection to prevent cancer recurrence.⁷⁸

Author information

Corresponding author

*E-mail: rotello@chem.umass.edu

Notes:

The authors declare no competing financial interest.

Acknowledgment

This work is supported by the National Institutes of Health EB022641 (V.M.R.), the National Science Foundation CHE-2108044 (R.W.V. and V.M.R), the National Institute of Environmental Health Sciences of the National Institutes of Health under award number U01ES026140 (DJJ) and the Department of Defense under contract #W81XWH-15-1-0217 (DJJ). C.-M.H. was partially supported by a fellowship from the University of Massachusetts as part of the Chemistry-Biology Interface Training Program (National Research Service Award T32 GM139789). The authors thank Dr. Amy S. Burnside from Flow Cytometry Core Facility at UMass Amherst, and Dr. James Chambers from Light Microscopy Core Facility at UMass Amherst.

Associated Content

Supporting Information

Electronic supporting information (ESI) is available free of charge at DOI: xxxx.

The synthesis and characterization of the materials used – nanoparticle, nanozyme, pro-Rho, pro-5FU, pro-HCA; cytotoxicity and cell uptake of nanozymes; therapeutic window between 5FU and pro-5FU; activation of pro-HCA in solution and in cells; tumor image for ICP-MS and after treatment; body weight of mice during and after the treatment.

References

¹ J.B. Wolinsky, Y.L. Colson, M.W. Grinstaff, Local drug delivery strategies for cancer treatment: Gels, nanoparticles, polymeric films, rods, and wafers, J. Control. Release. 159 (2012) 14–26. doi:10.1016/j.jconrel.2011.11.031.

² J. Conde, N. Oliva, Y. Zhang, N. Artzi, Local triple-combination therapy results in tumour regression and prevents recurrence in a colon cancer model, Nat. Mater. 15 (2016) 1128–1138. doi:10.1038/nmat4707.

³ R. Liu, R. Zuo, G.A. Hudalla, Harnessing molecular recognition for localized drug delivery, Adv. Drug Deliv. Rev. 170 (2021) 238–260. doi:10.1016/j.addr.2021.01.008.

⁴ D.B. Cheng, X.H. Zhang, Y.J. Gao, D. Wang, L. Wang, H. Chen, Z.Y. Qiao, H. Wang, Site-Specific Construction of Long-Term Drug Depot for Suppression of Tumor Recurrence, Small. 15 (2019). doi:10.1002/smll.201901813.

⁵ N. Bhattarai, J. Gunn, M. Zhang, Chitosan-based hydrogels for controlled, localized drug delivery, Adv. Drug Deliv. Rev. 62 (2010) 83–99. doi:10.1016/j.addr.2009.07.019.

⁶ D. Peer, J.M. Karp, S. Hong, O.C. Farokhzad, R. Margalit, R. Langer, Nanocarriers as an emerging platform for cancer therapy, Nat. Nanotechnol. 2 (2007) 751–760. doi:10.1038/nnano.2007.387.

⁷ D. Wen, G. Chen, Q. Chen, P.Y. Li, H. Cheng, Z. Gu, Engineering Protein Delivery Depots for Cancer Immunotherapy, Bioconjug. Chem. 30 (2019) 515–524. doi:10.1021/acs.bioconjchem.9b00061.

⁸ J.S. Basuki, F. Qie, X. Mulet, R. Suryadinata, A. V Vashi, Y.Y. Peng, L. Li, X. Hao, T. Tan, T.C. Hughes, Photo-Modulated Therapeutic Protein Release from a Hydrogel Depot Using Visible Light, Angew. Chemie. 129 (2017) 986–991. doi:10.1002/ange.201610618.

⁹ S. Pal, N. Medatwal, S. Kumar, A. Kar, V. Komalla, P.S. Yavvari, D. Mishra, Z.A. Rizvi, S. Nandan, D. Malakar, M. Pillai, A. Awasthi, P. Das, R.D. Sharma, A. Srivastava, S. Sengupta, U. Dasgupta, A. Bajaj, A Localized Chimeric Hydrogel Therapy Combats Tumor Progression through Alteration of Sphingolipid Metabolism, ACS Cent. Sci. 5 (2019) 1648–1662. doi:10.1021/acscentsci.9b00551.

¹⁰ Y. Lu, A.A. Aimetti, R. Langer, Z. Gu, Bioresponsive materials, Nat. Rev. Mater. 2 (2017) 16075. doi:10.1038/natrevmats.2016.75.

¹¹ S. Mitragotri, P.A. Burke, R. Langer, Overcoming the challenges in administering biopharmaceuticals: formulation and delivery strategies, Nat. Rev. Drug Discov. 13 (2014) 655–672. doi:10.1038/nrd4363.

¹² X. Xie, J. Wang, L. Zhang, S. Zeng, X. Su, Q. Chen, Bioresorbable Depot for Sustained Release of Immunostimulatory Resiquimod in Suppressing Both Primary Triple-Negative Breast Tumors and Metastatic Occurrence, Bioconjug. Chem. 32 (2021) 1008–1016. doi:10.1021/acs.bioconjchem.1c00171.

¹³ H. Ruan, Q. Hu, D. Wen, Q. Chen, G. Chen, Y. Lu, J. Wang, A Dual-Bioresponsive Drug-Delivery Depot for Combination of Epigenetic Modulation and Immune Checkpoint Blockade, Adv. Mater. 31 (2019) 1806957. doi:10.1002/adma.201806957.

¹⁴ D. Wen, J. Wang, D. Wen, J. Wang, G. Van Den Driessche, Q. Chen, Y. Zhang, G. Chen, H. Li, J. Soto, M. Liu, M. Ohashi, Z. Wang, P. Abdou, Q. Hu, G. Dotti, S. Li, D. Fourches, Z. Gu, Adipocytes as Anticancer Drug Delivery Depot, Matter. 1 (2019) 1203–1214. doi:10.1016/j.matt.2019.08.007.

¹⁵ M.W. Tibbitt, J.E. Dahlman, R. Langer, Emerging Frontiers in Drug Delivery, J. Am. Chem. Soc. 138 (2016) 704–717. doi:10.1021/jacs.5b09974.

- ¹⁶ C.R. Bertozzi, A decade of bioorthogonal chemistry, Acc. Chem. Res. 44 (2011) 651–653. doi:10.1021/ar200193f.
- ¹⁷ J. Chen, K. Li, S.E. Bonson, S.C. Zimmerman, A Bioorthogonal Small Molecule Selective Polymeric "clickase," J. Am. Chem. Soc. 142 (2020) 13966–13973. doi:10.1021/jacs.0c06553.
- ¹⁸ W. Wang, X. Zhang, R. Huang, C.M. Hirschbiegel, H. Wang, Y. Ding, V.M. Rotello, In situ activation of therapeutics through bioorthogonal catalysis, Adv. Drug Deliv. Rev. 176 (2021) 113893. doi:10.1016/j.addr.2021.113893.
- ¹⁹ D.P. Nguyen, H.T.H. Nguyen, L.H. Do, Tools and Methods for Investigating Synthetic Metal-Catalyzed Reactions in Living Cells, ACS Catal. 11 (2021) 5148–5165. doi:10.1021/acscatal.1c00438.
- ²⁰ X. Zhang, R. Huang, S. Gopalakrishnan, R. Cao-milán, V.M. Rotello, Bioorthogonal Nanozymes: Progress towards Therapeutic Applications, Trends Chem. 1 (2019) 90–98. doi:10.1016/j.trechm.2019.02.006.
- ²¹ E. Latocheski, G.M. Dal Forno, T.M. Ferreira, B.L. Oliveira, G.J.L. Bernardes, J.B. Domingos, Mechanistic insights into transition metal-mediated bioorthogonal uncaging reactions, Chem. Soc. Rev. 49 (2020) 7710–7729. doi:10.1039/d0cs00630k.
- ²² Y. Liu, Y. Bai, Design and Engineering of Metal Catalysts for Bio-orthogonal Catalysis in Living Systems, ACS Appl. Bio Mater. 3 (2020) 4717–4746. doi:10.1021/acsabm.0c00581.
- ²³ Y. Brudno, M.J. Pezone, T.K. Snyder, O. Uzun, C.T. Moody, M. Aizenberg, D.J. Mooney, Replenishable drug depot to combat post-resection cancer recurrence, Biomaterials. 178 (2018) 373–382. doi:10.1016/j.biomaterials.2018.05.005.
- ²⁴ R. Walther, J. Rautio, A.N. Zelikin, Prodrugs in medicinal chemistry and enzyme prodrug therapies, Adv. Drug Deliv. Rev. 118 (2017) 65–77. doi:10.1016/j.addr.2017.06.013.
- ²⁵ J. Rautio, H. Kumpulainen, T. Heimbach, R. Oliyai, D. Oh, T. Järvinen, J. Savolainen, Prodrugs: Design and clinical applications, Nat. Rev. Drug Discov. 7 (2008) 255–270. doi:10.1038/nrd2468.
- ²⁶ J. Rautio, N.A. Meanwell, L. Di, M.J. Hageman, The expanding role of prodrugs in contemporary drug design and development, Nat. Rev. Drug Discov. 17 (2018) 559–587. doi:10.1038/nrd.2018.46.
- ²⁷ B. Fejerskov, M.T.J. Olesen, A.N. Zelikin, Substrate mediated enzyme prodrug therapy, Adv. Drug Deliv. Rev. 118 (2017) 24–34. doi:10.1016/j.addr.2017.04.013.
- ²⁸ J. Li, P.R. Chen, Development and application of bond cleavage reactions in bioorthogonal chemistry, Nat. Chem. Biol. 12 (2016) 129–137. doi:10.1038/nchembio.2024.
- ²⁹ S. V Chankeshwara, E. Indrigo, M. Bradley, Palladium-mediated chemistry in living cells, Curr. Opin. Chem. Biol. 21 (2014) 128–135. doi:10.1016/j.cbpa.2014.07.007.
- ³⁰ M.O.N. van de L'Isle, M.C. Ortega-Liebana, A. Unciti-Broceta, Transition metal catalysts for the bioorthogonal synthesis of bioactive agents, Curr. Opin. Chem. Biol. 61 (2021) 32–42. doi:10.1016/j.cbpa.2020.10.001.
- ³¹ J. Tu, M. Xu, R.M. Franzini, Dissociative Bioorthogonal Reactions, ChembioChem. 20 (2019) 1615–1627. doi:10.1002/cbic.201800810.
- ³² J. Clavadetscher, E. Indrigo, S. V. Chankeshwara, A. Lilienkampf, M. Bradley, In-Cell Dual Drug Synthesis by Cancer-Targeting Palladium Catalysts, Angew. Chemie Int. Ed. 56 (2017) 6864–6868. doi:10.1002/anie.201702404.
- ³³ M. Sancho-albero, B. Rubio-ruiz, A.M. Pérez-lópez, V. Sebastián, P. Martín-duque, M. Arruebo, J. Santamaría, A. Unciti-broceta, Cancer-derived exosomes loaded with ultrathin palladium nanosheets for targeted bioorthogonal catalysis, Nat. Catal. 2 (2019) 864–872. doi:10.1038/s41929-019-0333-4.
- ³⁴ R.M. Yusop, A. Unciti-Broceta, E.M. V Johansson, R.M. Sánchez-Martín, M. Bradley, Palladium-mediated intracellular chemistry, Nat. Chem. 3 (2011) 239–243. doi:10.1038/nchem.981.
- ³⁵ F. Wang, Y. Zhang, Z. Du, J. Ren, X. Qu, Designed heterogeneous palladium catalysts for reversible light-controlled bioorthogonal catalysis in living cells, Nat. Commun. 9 (2018) 1209. doi:10.1038/s41467-018-03617-x.
- ³⁶ Z. Du, C. Liu, H. Song, P. Scott, Z. Liu, J. Ren, X. Qu, Neutrophil-Membrane-Directed Bioorthogonal Synthesis of Inflammation-Targeting Chiral Drugs, Chem. 6 (2020) 2060–2072. doi:10.1016/j.chempr.2020.06.002.
- ³⁷ S. Eda, I. Nasibullin, K. Vong, N. Kudo, M. Yoshida, A. Kurbangalieva, K. Tanaka, Biocompatibility and therapeutic potential of glycosylated albumin artificial metalloenzymes, Nat. Catal. 2 (2019) 780–792. doi:10.1038/s41929-019-0317-4.
- ³⁸ B. Lozhkin, T.R. Ward, Bioorthogonal strategies for the in vivo synthesis or release of drugs, Bioorganic Med. Chem. 45 (2021) 116310. doi:10.1016/j.bmc.2021.116310.

- ³⁹ G.Y. Tonga, Y. Jeong, B. Duncan, T. Mizuhara, R. Mout, R. Das, S.T. Kim, Y.C. Yeh, B. Yan, S. Hou, V.M. Rotello, Supramolecular regulation of bioorthogonal catalysis in cells using nanoparticle-embedded transition metal catalysts, Nat. Chem. 7 (2015) 597–603. doi:10.1038/nchem.2284.
- ⁴⁰ X. Zhang, S. Fedeli, S. Gopalakrishnan, R. Huang, A. Gupta, D.C. Luther, V.M. Rotello, Protection and Isolation of Bioorthogonal Metal Catalysts by Using Monolayer-Coated Nanozymes, ChemBioChem. 21 (2020) 2759–2763. doi:10.1002/cbic.202000207.
- ⁴¹ X. Źhang, R.F. Landis, P. Keshri, R. Cao-Milán, D.C. Luther, S. Gopalakrishnan, Y. Liu, R. Huang, G. Li, M. Malassiné, I. Uddin, B. Rondon, V.M. Rotello, Intracellular Activation of Anticancer Therapeutics Using Polymeric Bioorthogonal Nanocatalysts, Adv. Healthc. Mater. 10 (2021) 2001627. doi:10.1002/adhm.202001627.
- ⁴² Y. Huang, J. Ren, X. Qu, Nanozymes: Classification, Catalytic Mechanisms, Activity Regulation, and Applications, Chem. Rev. 119 (2019) 4357–4412. doi:10.1021/acs.chemrev.8b00672.
- ⁴³ J. Wu, X. Wang, Q. Wang, Z. Lou, S. Li, Y. Zhu, L. Qin, H. Wei, Nanomaterials with enzyme-like characteristics (nanozymes): next-generation artificial enzymes (II), Chem. Soc. Rev. 48 (2019) 1004–1076. doi:10.1039/c8cs00457a.
- ⁴⁴ R. Huang, C. Li, R. Cao-milan, L.D. He, J.M. Makabenta, X. Zhang, E. Yu, V.M. Rotello, Polymer-Based Bioorthogonal Nanocatalysts for the Treatment of Bacterial Biofilms, J. Am. Chem. Soc. 142 (2020) 10723–10729. doi:10.1021/jacs.0c01758.
- ⁴⁵ R. Cao-milan, S. Gopalakrishnan, L.D. He, R. Huang, L. Wang, L. Castellanos, D.C. Luther, R.F. Landis, J.M. V Makabenta, C. Li, X. Zhang, F. Scaletti, R.W. Vachet, V.M. Rotello, Thermally Gated Bio-orthogonal Nanozymes with Supramolecularly Confined Porphyrin Catalysts for Antimicrobial Uses, Chem. 6 (2020) 1–12. doi:10.1016/j.chempr.2020.01.015.
- ⁴⁶ X. Zhang, Y. Liu, S. Gopalakrishnan, L. Castellanos-Garcia, G. Li, M. Malassiné, I. Uddin, R. Huang, D. Luther, R. Vachet, V. Rotello, Intracellular Activation of Bioorthogonal Nanozymes through Endosomal Proteolysis of the Protein Corona, ACS Nano. 14 (2020) 4767–4773. doi:10.1021/acsnano.0c00629.
- ⁴⁷ X. Zhang, S. Lin, R. Huang, A. Gupta, S. Fedeli, R. Cao-mil, D.C. Luther, Y. Liu, M. Jiang, G. Li, B. Rondon, H. Wei, V.M. Rotello, Degradable ZnS-Supported Bioorthogonal Nanozymes with Enhanced Catalytic Activity for Intracellular Activation of Therapeutics, J. Am. Chem. Soc. 144 (2022) 12893–12900. doi:10.1021/jacs.2c04571..
- ⁴⁸ R. Das, R.F. Landis, G.Y. Tonga, R. Cao-Milán, D.C. Luther, V.M. Rotello, Control of Intra- versus Extracellular Bioorthogonal Catalysis Using Surface-Engineered Nanozymes, ACS Nano. 13 (2019) 229–235. doi:10.1021/acsnano.8b05370.
- ⁴⁹ A. Gupta, R. Das, G. Yesilbag Tonga, T. Mizuhara, V.M. Rotello, Charge-Switchable Nanozymes for Bioorthogonal Imaging of Biofilm-Associated Infections, ACS Nano. 12 (2018) 89–94. doi:10.1021/acsnano.7b07496.
- ⁵⁰ A. Gupta, R. Das, J.M. Makabenta, A. Gupta, X. Zhang, T. Jeon, R. Huang, Y. Liu, S. Gopalakrishnan, R.C. Milán, V.M. Rotello, Erythrocyte-mediated delivery of bioorthogonal nanozymes for selective targeting of bacterial infections, Mater. Horizons. 8 (2021) 3424–3431. doi:10.1039/d1mh01408k.
- ⁵¹ J. Hardie, J.M. Makabenta, A. Gupta, R. Huang, R. Cao-Milán, R. Goswami, X. Zhang, P. Abdulpurkar, M.E. Farkas, V.M. Rotello, Selective treatment of intracellular bacterial infections using host cell-targeted bioorthogonal nanozymes, Mater. Horizons. 9 (2022) 1489–1494. doi:10.1039/D1MH02042K.
- ⁵² M.A. Miller, B. Askevold, H. Mikula, R.H. Kohler, D. Pirovich, R. Weissleder, Nano-palladium is a cellular catalyst for in vivo chemistry, Nat. Commun. 8 (2017) 15906. doi:10.1038/ncomms15906.
- ⁵³ M.A. Miller, H. Mikula, G. Luthria, R. Li, S. Kronister, M. Prytyskach, R.H. Kohler, T. Mitchison, R. Weissleder, Modular Nanoparticulate Prodrug Design Enables Efficient Treatment of Solid Tumors Using Bioorthogonal Activation, ACS Nano. 12 (2018) 12814–12826. doi:10.1021/acsnano.8b07954.
- ⁵⁴ Z. Chen, H. Li, Y. Bian, Z. Wang, G. Chen, X. Zhang, Y. Miao, D. Wen, J. Wang, G. Wan, Y. Zeng, P. Abdou, J. Fang, S. Li, C.-J. Sun, Z. Gu, Bioorthogonal catalytic patch, Nat. Nanotechnol. 16 (2021) 933–941. doi:10.1038/s41565-021-00910-7.
- ⁵⁵ M. Hoop, A.S. Ribeiro, D. Rösch, P. Weinand, N. Mendes, F. Mushtaq, X. Chen, Y. Shen, C.F. Pujante, J. Puigmartí-luis, J. Paredes, B.J. Nelson, A.P. Pêgo, S. Pané, Mobile Magnetic Nanocatalysts for Bioorthogonal Targeted Cancer Therapy, Adv. Funct. Mater. 28 (2018) 1705920. doi:10.1002/adfm.201705920.
- ⁵⁶ C. Adam, T.L. Bray, A.M. Pérez-López, E.H. Tan, B. Rubio-Ruiz, D.J. Baillache, D.R. Houston, M.J. Salji, H.Y. Leung, A. Unciti-Broceta, A 5-FU Precursor Designed to Evade Anabolic and Catabolic Drug Pathways

- and Activated by Pd Chemistry in Vitro and in Vivo, J. Med. Chem. 65 (2022) 552–561. doi:10.1021/acs.jmedchem.1c01733.
- ⁵⁷ S. Fedeli, J. Im, S. Gopalakrishnan, J.L. Elia, A. Gupta, D. Kim, V.M. Rotello, Nanomaterial-based bioorthogonal nanozymes for biological applications, Chem. Soc. Rev. 50 (2021) 13467–13480. doi:10.1039/d0cs00659a.
- ⁵⁸ R. Cao-Milán, L.D. He, S. Shorkey, G.Y. Tonga, L.S. Wang, X. Zhang, I. Uddin, R. Das, M. Sulak, V.M. Rotello, Modulating the catalytic activity of enzyme-like nanoparticles through their surface functionalization, Mol. Syst. Des. Eng. 2 (2017) 624–628. doi:10.1039/c7me00055c.
- ⁵⁹ L.J. Castellanos-García, S. Gokhan Elci, R.W. Vachet, Reconstruction, analysis, and segmentation of LA-ICP-MS imaging data using Python for the identification of sub-organ regions in tissues, Analyst. 145 (2020) 3705–3712. doi:10.1039/c9an02472g.
- ⁶⁰ Z.-J. Zhu, R. Tang, Y.-C. Yeh, O.R. Miranda, V.M. Rotello, R.W. Vachet, Determination of the Intracellular Stability of Gold Nanoparticle Monolayers Using Mass Spectrometry, Anal. Chem. 84 (2012), 4321–4326. doi:10.1021/ac203408v.
- ⁶¹ C.A. Lochbaum, A.K. Chew, X. Zhang, V.M. Rotello, R.C. Van Lehn, J.A. Pedersen, Lipophilicity of Cationic Ligands Promotes Irreversible Adsorption of Nanoparticles to Lipid Bilayers, ACS Nano. 15 (2021) 6562–6572. doi:10.1021/acsnano.0c09732.
- ⁶² R. Das, J. Hardie, B.P. Joshi, X. Zhang, A. Gupta, D.C. Luther, S. Fedeli, M.E. Farkas, V.M. Rotello, Macrophage-Encapsulated Bioorthogonal Nanozymes for Targeting Cancer Cells, JACS Au. 2 (2022) 1679–1685. doi:10.1021/jacsau.2c00247.
- ⁶³ Y. Jiang, S. Huo, T. Mizuhara, R. Das, Y.W. Lee, S. Hou, D.F. Moyano, B. Duncan, X.J. Liang, V.M. Rotello, The Interplay of Size and Surface Functionality on the Cellular Uptake of Sub-10 nm Gold Nanoparticles, ACS Nano. 9 (2015) 9986–9993. doi:10.1021/acsnano.5b03521.
- ⁶⁴ C.S. Kim, N.D.B. Le, Y. Xing, B. Yan, C. Kim, R.W. Vachet, V.M. Rotello, The Role of Surface Functionality in Nanoparticle Exocytosis, Adv. Healthc. Mater. 3 (2014) 1200–1202. doi:10.1002/adhm.201400001.
- ⁶⁵ S.G. Elci, Y. Jiang, B. Yan, S.T. Kim, K. Saha, D.F. Moyano, L.C. Jackson, V.M. Rotello, R.W. Vachet, Surface Charge Controls the Suborgan Biodistributions of Gold Nanoparticles, ACS Nano. 10 (2016) 5536–5542. doi:10.1021/acsnano.6b02086.
- ⁶⁶ R.R. Arvizo, O.R. Miranda, D.F. Moyano, C.A. Walden, K. Giri, J.D. Robertson, V.M. Rotello, J.M. Reid, P. Mukherjee, Modulating Pharmacokinetics, Tumor Uptake and Biodistribution by Engineered Nanoparticles, PLoS One. 6 (2011) e24374. doi:10.1371/journal.pone.0024374.
- ⁶⁷ B. Li, P. Liu, H. Wu, X. Xie, Z. Chen, F. Zeng, S. Wu, A bioorthogonal nanosystem for imaging and in vivo tumor inhibition, Biomaterials. 138 (2017) 57–68. doi:10.1016/j.biomaterials.2017.05.036.
- ⁶⁸ X. He, L. Li, Y. Fang, W. Shi, X. Li, H. Ma, In vivo imaging of leucine aminopeptidase activity in drug-induced liver injury and liver cancer via a near-infrared fluorescent probe, Chem. Sci. 8 (2017) 3479–3483. doi:10.1039/c6sc05712h.
- ⁶⁹ S. Hou, K.N. Sikora, R. Tang, Y. Liu, Y.W. Lee, S.T. Kim, Z. Jiang, R.W. Vachet, V.M. Rotello, Quantitative Differentiation of Cell Surface-Bound and Internalized Cationic Gold Nanoparticles Using Mass Spectrometry, ACS Nano. 10 (2016) 6731–6736. doi:10.1021/acsnano.6b02105.
- ⁷⁰ D.B. Longley, D.P. Harkin, P.G. Johnston, 5-FLUOROURACIL: MECHANISMS OF ACTION AND CLINICAL STRATEGIES, Nat. Rev. Cancer. 3 (2003) 330–338. doi:10.1038/nrc1074.
- ⁷¹ J.L. Grem, 5-Fluoropyrimidines. In: B.A. Chabner, D.L. Longo, editors. Cancer Chemotherapy and Biotherapy. 2nd ed. Philadelphia, PA: Lippincott-Raven; 1996 (ISBN 0397514182). p. 146-211.
- ⁷² F. Alessandrino, L. Qin, G. Cruz, S. Sahu, M. H. Rosenthal, J. A. Meyerhardt, A. B. Shinagare, 5-Fluorouracil Induced Liver Toxicity in Patients with Colorectal Cancer: Role of Computed Tomography Texture Analysis as a Potential Biomarker. Abdom. Radiol. 44 (2019), 3099–3106.doi: 10.1007/s00261-019-02110-3
- ⁷³ M.W. Saif, A. Choma, S.J. Salamone, E. Chu, Pharmacokinetically Guided Dose Adjustment of 5-Fluorouracil: A Rational Approach to Improving Therapeutic Outcomes, J. Natl. Cancer Inst. 101 (2009) 1543–1552. doi:10.1093/jnci/djp328.
- ⁷⁴ J.T. Weiss, J.C. Dawson, K.G. Macleod, W. Rybski, C. Fraser, C. Torres-Sánchez, E.E. Patton, M. Bradley, N.O. Carragher, A. Unciti-Broceta, Extracellular palladium-catalysed dealkylation of 5-fluoro-1-propargyl-uracil as a bioorthogonally activated prodrug approach, Nat. Commun. 5 (2014) 3277. doi:10.1038/ncomms4277. 1543–1552. doi:10.1093/jnci/djp328.

⁷⁵ D.R. Vogus, M.A. Evans, A. Pusuluri, A. Barajas, M. Zhang, V. Krishnan, M. Nowak, S. Menegatti, M.E. Helgeson, T.M. Squires, S. Mitragotri, A hyaluronic acid conjugate engineered to synergistically and sequentially deliver gemcitabine and doxorubicin to treat triple negative breast cancer, J. Control. Release. 267 (2017) 191–202. doi:10.1016/j.jconrel.2017.08.016.

⁷⁶ S.G. Elci, B. Yan, S.T. Kim, C.S. Kim, Y. Jiang, K. Saha, D.F. Moyano, A.L.M. Marsico, V.M. Rotello, R.W. Vachet, Dual-Mode Mass Spectrometric Imaging for Dtermination of in Vivo Stability of Nanoparticle Monolayers, ACS Nano. 11 (2017) 7424–7430. doi:10.1021/acsnano.7b03711.

⁷⁷ B. R. Thapa, A. Walia, Liver function tests and their interpretation. *Indian J Pediatr* 74 (2007), 663-671. doi: 10.1007/s12098-007-0118-7.

⁷⁸ J.K. Anninga, H. Gelderblom, M. Fiocco, J.R. Kroep, A.H.M. Taminiau, P.C.W. Hogendoorn, R.M. Egeler, Chemotherapeutic adjuvant treatment for osteosarcoma: Where do we stand? *Eur. J. Cancer* 47 (2011), 2431-2445. doi: 10.1016/j.ejca.2011.05.030.